

Geophysical Research Letters®

RESEARCH LETTER

10.1029/2022GL102032

Key Points:

- The frequency of MHWs showed an insignificant trend, and the duration, intensity, area and moving distance increased greatly over 1982–2020
- The strongest MHWs (more than the 80th percentile) have the largest increase in moving distance
- The extreme MHW category dominates the increase in projection/total area due to the rising moving distance

Supporting Information:

Supporting Information may be found in the online version of this article.

Correspondence to:

Y. He,
heyongli@lzu.edu.cn

Citation:

He, Y., Zhang, B., Xia, Z., Wang, S., & Guan, X. (2023). Global warming has increased the distance traveled by marine heatwaves. *Geophysical Research Letters*, 50, e2022GL102032. <https://doi.org/10.1029/2022GL102032>

Received 5 NOV 2022

Accepted 12 JAN 2023



Author Contributions:

Conceptualization: Yongli He
Formal analysis: Yongli He, Boyuan Zhang, Zihan Xia
Funding acquisition: Xiaodan Guan
Investigation: Boyuan Zhang, Zihan Xia
Methodology: Yongli He
Software: Boyuan Zhang, Zihan Xia
Supervision: Yongli He
Visualization: Boyuan Zhang, Zihan Xia
Writing – original draft: Yongli He, Boyuan Zhang
Writing – review & editing: Yongli He, Boyuan Zhang, Shanshan Wang, Xiaodan Guan

© 2023. The Authors.

This is an open access article under the terms of the [Creative Commons Attribution License](https://creativecommons.org/licenses/by/4.0/), which permits use, distribution and reproduction in any medium, provided the original work is properly cited.

Global Warming has Increased the Distance Traveled by Marine Heatwaves

Yongli He^{1,2} , Boyuan Zhang¹, Zihan Xia¹, Shanshan Wang¹, and Xiaodan Guan^{1,2} 

¹Key Laboratory for Semi-Arid Climate Change of the Ministry of Education, College of Atmospheric Sciences, Lanzhou University, Lanzhou, China, ²Collaborative Innovation Center for Western Ecological Safety, Lanzhou, China

Abstract Due to the destructive effects of marine heatwaves (MHWs) on marine ecosystems and local economies, whether they become more frequent and stronger under global warming has attracted much attention. The proposed event-based algorithm identifies 3,843 MHWs during 1982–2020. Except for the MHW frequency, the global averaged duration, intensity, area and moving distance increased significantly. The contributions of the frequency and mean projection area to the total projection area were further investigated from the four categories of MHWs. The results showed that for moderate MHWs, frequency contributes more than the mean projection area to the increase in projection area; however, for strong, severe, and extreme MHWs, the mean projection area contributes much more than frequency. Due to the increased moving distance, the projected area change of the extreme MHW dominates the increase in the total projected area. The high sensitivity of extreme MHWs to global warming deserves extra attention.

Plain Language Summary Marine heatwaves (MHWs), which are characterized by temperatures exceeding a specific threshold for an extended period, have a severe impact on marine ecology and societal economics. Previous studies assumed that MHWs will become longer, more frequent, and more intense under global warming, but they ignored the movement of MHWs caused by ocean currents. Here, we use a three-dimensional connected detection algorithm to track the spatiotemporal connection of MHWs across the globe over 1982–2020. The results show that global averages for MHW duration, intensity, area, and total distance have increased significantly except for MHW moving speed, frequency and area mean intensity. We find that stronger MHWs have a longer traveling distance and a larger affection area. As the total projection area is divided into the mean projection area and frequency, we further investigate the contribution of the frequency and mean projection area to the trend of the total projection area at different MHW intensities. We find that frequency contributes more to the increase in total projection area in weaker MHWs, while mean projection area contributes more in stronger MHWs. It is necessary to consider the movement of MHWs when predicting future changes in MHWs.

1. Introduction

A phenomenon known as marine heatwave (MHW), characterized by a prolonged period of excessive warmth, has devastating impacts on the biodiversity loss of marine species (Smale et al., 2019; Wernberg et al., 2012, 2016), coral reef bleaching (Hughes et al., 2017; Mohanty et al., 2021), and fishing management (Caputi et al., 2016; Cheung & Frölicher, 2020; Mills et al., 2013). For example, the northern Great Barrier Reef experienced anomalous temperatures in the summers of 2016 and 2017, leading to back-to-back mass bleaching of corals (Hughes et al., 2018). On the other hand, MHWs were demonstrated to dramatically strengthen atmospheric blocking by providing a diabatic source of wave activity flux, as observed in the Pacific Northwest (Neal et al., 2022). Therefore, it is important to understand the response of MHWs to global warming.

The temporal and spatial characteristics of MHWs have been extensively assessed at various worldwide locations and times (Benthuisen et al., 2018; Galli et al., 2017; Holbrook et al., 2022; Liang et al., 2017; Liu et al., 2022; Manta et al., 2018; Sparnocchia et al., 2006; Yao & Wang, 2021). For example, MHWs lasted for 251 days from 2015 to 2016 and reached a maximum intensity of 2.9°C above the climatology over the Tasman Sea (Oliver et al., 2017). A total of 426 MHWs were identified over the west coast of South America from 1982 to 2019, which lasted from 5 to 610 days and spatially covered 625–5,625,000 km² (Pietri et al., 2021). On a global scale, MHW duration and intensity increased by 84% and 65%, respectively, between 1982–1998 and 2000–2016 (Oliver et al., 2018). Based on satellite observations and a suite of Earth system models, the spatial extent of

MHWs is 21 times larger than that in preindustrial times (Frölicher et al., 2018). The CMIP5 models projected that MHW metrics will continue to increase in the future and that the ocean will enter a permanent MHW state by the end of the 21st century (Oliver et al., 2019). However, most of these studies solely assess MHW metrics based on temporal or spatial changes, ignoring the spatiotemporal continuity of MHWs.

Due to the flow of ocean currents, the development and extinction of MHWs are associated with the merging and fragmentation of sea surface temperature anomalies at different grids, thus exhibiting spatial and temporal continuity. Due to the rise in temperature, marine species change their distribution to find a suitable habitat (Jacox et al., 2020; Walker et al., 2020). Therefore, moving MHWs have a significant impact on the habitats of marine species. For example, due to the southward migration of planktonic krill during the MHW period, whale sharks move further south of their original home (Pearce & Feng, 2013). On the other hand, the flow of ocean currents plays an important role in the evolution of MHWs (Elzahaby et al., 2021; Holbrook et al., 2019; Oliver et al., 2017). For example, the southward flow of the East Australian Current dominated the evolution of the MHW over the Tasman Sea in 2015/16 (Oliver et al., 2017). Ocean currents are accelerating under global warming (Hu et al., 2020). However, whether the accelerated currents influence the movements of MHWs remains unknown and cannot be solved from a grid perspective. Therefore, to investigate the response of large-scale MHW events to global warming, it is necessary to consider the movement of MHWs.

Recent studies have developed a three-dimensional (3-D) connected component algorithm, also called the event-based algorithm, to detect atmospheric blocking or land heatwaves by tracking spatiotemporal continuity (Fang & Lu, 2020; Luo, Lau, et al., 2022; Schwierz et al., 2004; Steinfeld & Pfahl, 2019; Steinfeld et al., 2020, 2022; Vogel et al., 2020). For instance, Luo, Lau, et al. (2022) studied the spatiotemporal evolution of contiguous heatwaves in China and found that the frequency, magnitude, and traveling distance across China are increasing. Reddy et al. (2021) examine contiguous heatwaves over Australia and find that heatwaves are becoming more extensive and lasting longer than in the historical period. However, these metrics related to 3-D MHW events remain undetermined, and the response of these metrics to global warming remains unknown.

In this study, we detect MHWs using an event-based algorithm from a 3D perspective based on the NOAA OI SSTv2.0 data set from 1982 to 2020 and explore the response of MHWs to multiple metrics of global warming, including duration, frequency, intensity, area and movement metrics. This analysis will provide an understanding of the observed changes in the multiple metrics of MHWs and the underlying mechanism for these changes.

2. Methods

2.1. Sea Surface Temperature Data

The sea surface temperature (SST) data and sea ice data used in this study were derived from the National Oceanic and Atmospheric Administration (NOAA) Optimum Interpolation Sea Surface Temperature (OISST) V2.0 high-resolution gridded data set (Reynolds et al., 2007). The daily SST covers the period from 1982 to 2020 with a spatial resolution of $0.25^\circ \times 0.25^\circ$, generated from the Advanced Very High Resolution Radiometer (AVHRR). To exclude the impact of sea ice, only grid cells without sea ice cover were used in the study.

2.2. 3D-Connected Detection Algorithm of Marine Heatwaves and Its Metrics

Compared to the event-based algorithm, we referred to the conventional MHW detection algorithm as the grid-based detection algorithm provided by Oliver et al. (2018), with the definition of MHWs as discrete prolonged anomalously warm events (Hobday et al., 2016). Discrete is defined quantitatively as an event with identified start and end dates, prolonged means MHW duration for at least 5 days and anomalously signifies that the intensity of MHW exceeds the seasonally varying 90th threshold. The seasonally varying threshold allows MHW occurrence at any time of the year, with a higher threshold in summer and a lower threshold in winter.

Therefore, we applied a three-dimensional connected (3D-connected) MHW detection algorithm, taking into account the continuous movement of ocean currents. We also define an MHW as a discrete prolonged anomalously warm event. The meaning of prolonged and anomalous is the same as Hobday et al., 2016, but the definition of discrete has changed, which is defined as an event not only with identified start and end dates but also with a well-defined boundary. The main steps of the 3D-connected algorithm are illustrated in Figure S1 in Supporting Information S1: (a) Threshold: the seasonally varying 90th percentile was calculated for each day of the year within an 11-day window centered on the day and then smoothed by a 31-day moving average, as in Hobday et al. (2016). (b) Determine

connection: for each day, the connectivity of the two-dimensional temperature field is determined. The region where the two-dimensional temperature field exceeds the threshold and connects with the adjacent grids is recorded as a single event. (c) Overlap limit: only two connected areas with overlap ratios greater than 50% at two consecutive time-steps are preserved, while the remainder are eliminated. (d) Persistence limit: First, MHW events were determined by 3D connection with a 10-connected structure (Figure S2b in Supporting Information S1). The persistence of each event is computed, and only those events lasting more than 5 days are preserved. (e) Area limit: the projection area of each event is computed, and only those events with a projection area greater than 10^6 km^2 are selected to eliminate small area events (Luo, Lau, et al., 2022). A complete MHW event is detected through the above steps, and then the metrics of each MHW event are diagnosed. Their definitions are provided in Table S1 in Supporting Information S1, consistent with previous studies (Luo, Lau, et al., 2022, 2022b). The associated annual MHW metrics are also calculated. Note that if the annual MHW metrics are across multiple years, MHW metrics are assigned to every year. Despite the possibility of inaccuracy if MHWs span multiple years, the MHW duration is typically less than 100 days (Figure S3c in Supporting Information S1). Therefore, multiyear MHW is uncommon and this inaccuracy can be ignored.

Previous studies have demonstrated that the event-based algorithm is insensitive to the choice of parameters (Luo, Lau, et al., 2022; Schwierz et al., 2004; Steinfeld et al., 2020, 2022; Steinfeld & Pfahl, 2019). Therefore, the parameters are as follows: overlap ratio (50%), duration (5 days) and area limit (10^6 km^2). It should be noted that the 10-connected structure is a stricter limitation on connection than the 26-connected structure, and the choice of 10-connected and 26-connected components may affect the final results (Figure S2 and Text S1 in Supporting Information S1). Large-scale MHW events cannot move so quickly that there is no overlap between successive daily time steps. Therefore, a 26-connected structure is insufficient for detecting large-sale MHW events. We think that MHWs should be identified at an earlier stage of their life cycle; therefore, the area limit should be determined after other steps to preserve the full evolution of the MHW event. The MHW event at the boundary should be regarded as a single event because the Earth is spherical. We merged the two events across the boundary into one event before processing the overlap and persistence limit.

The MHW is divided into four categories (moderate, strong, severe, and extreme) based on the degree to which the temperature exceeds the baseline climatology on each grid (Hobday et al., 2018). The category of MHW events is calculated as the maximum value over the MHW event grid using the variables in Equation 1.

$$\text{category} = \frac{\text{sst} - \text{clim}}{\text{thresh} - \text{clim}} = \begin{cases} 1 \sim 2, & \text{moderate} \\ 2 \sim 3, & \text{strong} \\ 3 \sim 4, & \text{severe} \\ \geq 4, & \text{extreme} \end{cases} \quad (1)$$

where thresh and clim represent the 90th percentile threshold and climatological mean value of SST from 1982 to 2020, respectively.

2.3. The Contribution of Moving Distance to the Increase in Projection Area and Total Area

We use a weighted-averaged framework to evaluate the contributions of projection area trends in four categories to the total projection area trend (Du et al., 2020). The projection area can be expressed as the weighted average of the projection area in the four categories as follows:

$$S = f_1 \times S_1 + f_2 \times S_2 + f_3 \times S_3 + f_4 \times S_4 \quad (2)$$

where $f_1 \sim f_4$ represent the frequency of MHW events in the four categories and $S_1 \sim S_4$ represent the mean projection area of MHW events in the four categories.

With global warming, we assume that each variable in Equation 2 changes by a certain amount. Substituting into Equation 2 and taking the average for a long-term period, we obtain Equation 3.

$$\begin{aligned} \bar{S} &= \bar{f}_1 \times \bar{S}_1 + \bar{f}_2 \times \bar{S}_2 + \bar{f}_3 \times \bar{S}_3 + \bar{f}_4 \times \bar{S}_4 \\ &= \bar{f}_1 \times \bar{S}_1 + \bar{f}_2 \times \bar{S}_2 + \bar{f}_3 \times \bar{S}_3 + \bar{f}_4 \times \bar{S}_4 \\ &\quad + \Delta f_1 \times \Delta S_1 + \Delta f_2 \times \Delta S_2 + \Delta f_3 \times \Delta S_3 + \Delta f_4 \times \Delta S_4 \end{aligned} \quad (3)$$

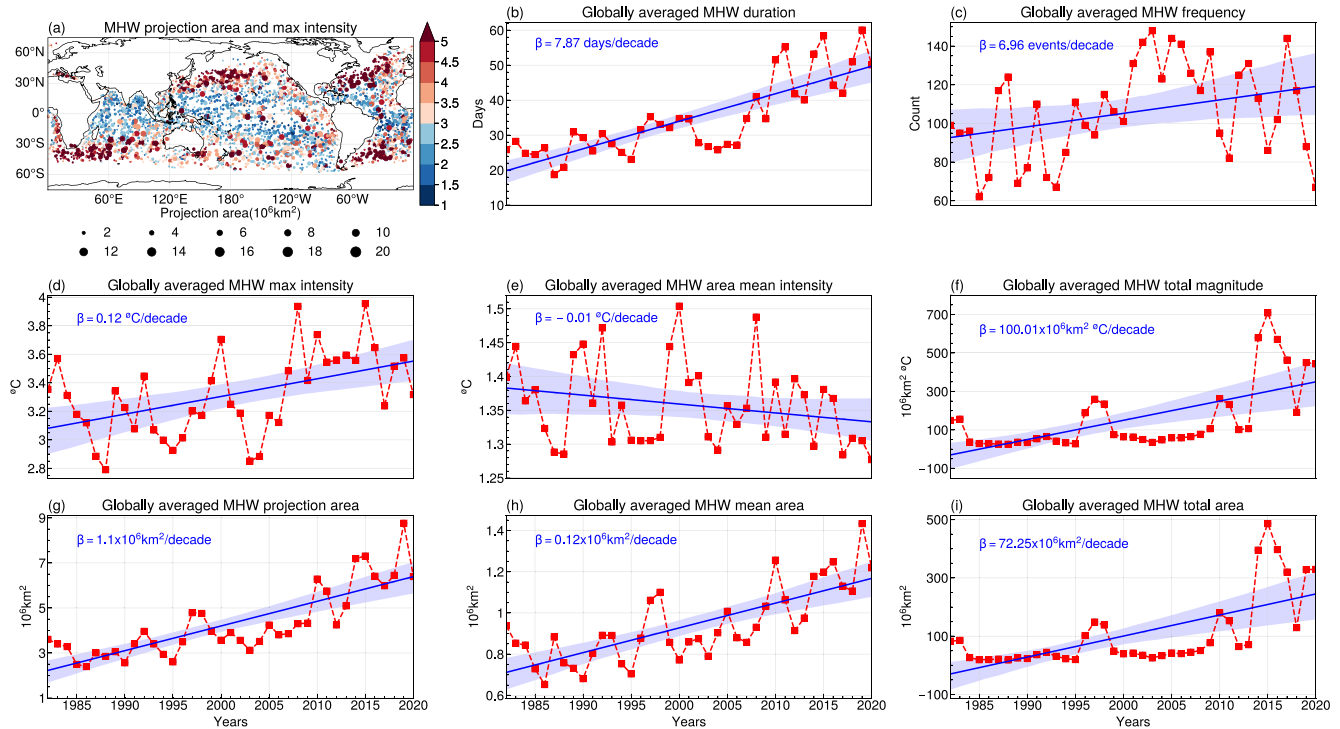


Figure 1. Global MHW properties. (a) Distribution of the overall centroids of MHWs during 1982–2020, with the dot color and size representing the intensity and projection area, respectively. Observed temporal variation in globally averaged multiple metrics of MHWs during 1982–2020, including duration (b), frequency (c), maximum intensity (d), area mean intensity (e), total magnitude (f), projection area (g), mean area (h) and total area (i). The blue lines represent the corresponding linear trend. The shaded area indicates the 95% confidence interval of the trend line. All trends are statistically significant at the 0.05 level, except for frequency and area mean intensity.

The variation of Equation 2 minus Equation 3 gives Equation 4.

$$\begin{aligned} \Delta S = & \overline{f_1} \times \Delta S_1 + \Delta f_1 \times \overline{S_1} + \left(\Delta f_1 \times \Delta S_1 - \overline{\Delta f_1 \times \Delta S_1} \right) \\ & + \overline{f_2} \times \Delta S_2 + \Delta f_2 \times \overline{S_2} + \left(\Delta f_2 \times \Delta S_2 - \overline{\Delta f_2 \times \Delta S_2} \right) \\ & + \overline{f_3} \times \Delta S_3 + \Delta f_3 \times \overline{S_3} + \left(\Delta f_3 \times \Delta S_3 - \overline{\Delta f_3 \times \Delta S_3} \right) \\ & + \overline{f_4} \times \Delta S_4 + \Delta f_4 \times \overline{S_4} + \left(\Delta f_4 \times \Delta S_4 - \overline{\Delta f_4 \times \Delta S_4} \right) \end{aligned} \quad (4)$$

The right side of Equation (4) comprises three terms for each category: $\overline{f_i} \times \Delta S_i$ is the area term, $\Delta f_i \times \overline{S_i}$ is the frequency term and $\left(\Delta f_i \times \Delta S_i - \overline{\Delta f_i \times \Delta S_i} \right)$ is the residual term, where subscript i is the index of the moderate, strong, severe and extreme categories. The total projection area changes are the sum of changes induced by the area term, frequency term and residual term. Based on this, the contribution of each term was calculated by the slope of each term at the right side divided by the slope of the left side of Equation (4). The analysis of the total area is the same as the above calculation.

3. Results and Discussion

3.1. The Response of Event-Based Detected MHWs

We applied a 3D-connected detection algorithm to detect MHWs from a 3-D perspective over 1982–2020. Following this algorithm, MHWs occur when they overlap with adjacent days, persist for at least 5 days, and affect an area of more than one million km^2 (detailed description in method 2.2). This method identifies 3843 MHW events globally during 1982–2020 (Figure 1a), and then determines the MHW duration, frequency, intensity metrics, area metrics, and movement characteristics for each event.

MHW metrics are significantly increasing under global warming (Figure 1). For the MHW duration and frequency metrics, the global average MHW duration increased significantly, with a trend of 7.87 days/decade, but the global MHW frequency increased at a rate of 6.96 events/decade, which did not pass the significance test. For the intensity metrics, the MHW maximum intensity and total magnitude increase at rates of $0.12^{\circ}\text{C}/\text{decade}$ and $100.01 \text{ million km}^2/\text{decade}$, respectively, but the area mean intensity decreases at a rate of $-0.01^{\circ}\text{C}/\text{decade}$. For area metrics, the projection area, mean area and total area expand significantly at rates of $1.1 \text{ million km}^2/\text{decade}$, $0.12 \text{ million km}^2/\text{decade}$ and $72.25 \text{ million km}^2/\text{decade}$, respectively.

It should be noted that the increase in MHW frequency is not significant, and the increasing trend of the duration of MHWs is much longer in the event-based method than in the grid-based method (Oliver et al., 2018). These inconsistencies may be caused by the movement of the MHWs. Due to the mobility of the ocean, although the MHW diminishes at this location, it indeed moves to the adjacent grid by the ocean current and occurs in a certain area. This movement can be captured by an event-based algorithm but cannot be detected by a traditional grid-based algorithm. Therefore, the event-based method causes a longer duration of MHW and an insignificant change in MHW frequency. The increasing frequency in the grid-based result was consistent with the increasing projection and total area in the event-based result, rather than frequency. The response of MHWs to global warming varies in different ocean basins (detailed description Text S4 and Figures S6–S10 in Supporting Information S1).

3.2. The Movement of MHWs

The linkage between the properties of MHW events is important for predicting combined changes in multiple properties of MHW events in the future. Therefore, the relationship between maximum intensity, moving distance, and projection area was further examined. The correlation coefficient between the total moving distance and projection area reaches 0.85 at the 0.01 significance level (Figure 2a). The correlation between the MHW maximum intensity and projection area is 0.45 at the 0.01 significance level (Figure 2c), indicating that the more intense the MHW is, the larger the region it will affect. Figure 2b depicts a correlation of 0.52 between total distance and maximum intensity at the 0.01 significance level, indicating that the more intense the MHW is, the further it will travel. Due to their strong relationship, we can anticipate that global warming will increase not only the maximum intensity (Figure 1d) but also the projection area and moving distance simultaneously (Figures 1g and 3a). Since the projection area is a function of the mean area and total distance, and the total distance is a function of the moving speed and duration, we further investigate the link between the above metrics (detailed description in Text S3 and Figure S5 in Supporting Information S1).

Due to intensified wind, ocean currents are accelerated under global warming (Hu et al., 2020). However, the MHW moving distance and moving speed respond differently to the acceleration of ocean currents. Moving distance increases significantly at a rate of $1,696.32 \text{ km}/\text{decade}$ (Figure 3a), while moving speed decreases insignificantly at a rate of $-1.69 \text{ km}/\text{day}/\text{decade}$ (Figure 3b). To explore the contrast response of moving metrics under global warming, MHW movement metrics are divided into 40 percentile bins based on MHW category bins, calculated as follows. The MHW intensity category was first ranked from small to high, and then MHW moving metrics were assigned into 40 bins. Then, the trend of the MHW moving metrics inside each bin was calculated using a linear least squares fit. The results indicate that the MHW moving distance exhibits an increasing trend in most bins (Figure 3c), but the moving speed of MHWs shows a divergent trend in most percentile bins, which does not pass the significance test except for two bins (Figure 3d). Due to the positive correlation between maximum intensity and moving distance (Figure 2b), the largest increase in moving distance occurred in the percentile bins greater than 80%, but the increasing trend of moving distance in the intensity bins below 40% was not significant. The results imply that the current speed did not accelerate during the MHW event period and that the increase in total moving distance under global warming was not caused by moving speed but rather by an increase in the MHW duration (Figures 1b and 3a).

Interestingly, the insignificant decrease in the MHW moving speed is inconsistent with the acceleration of ocean currents, which is induced by the intensification of surface winds (Hu et al., 2020). Intensified wind not only accelerates the ocean current but also has enough energy to break ocean stratification. Reduced stratification will increase the vertical mixing of the ocean, which will deepen the mixing layer. Because the sea surface temperature is higher than that of deep ocean, increasing the depth of the mixing layer will cool the ocean surface and reduce the SST variability, resulting in a smaller sea surface temperature anomaly than the shallow mixing

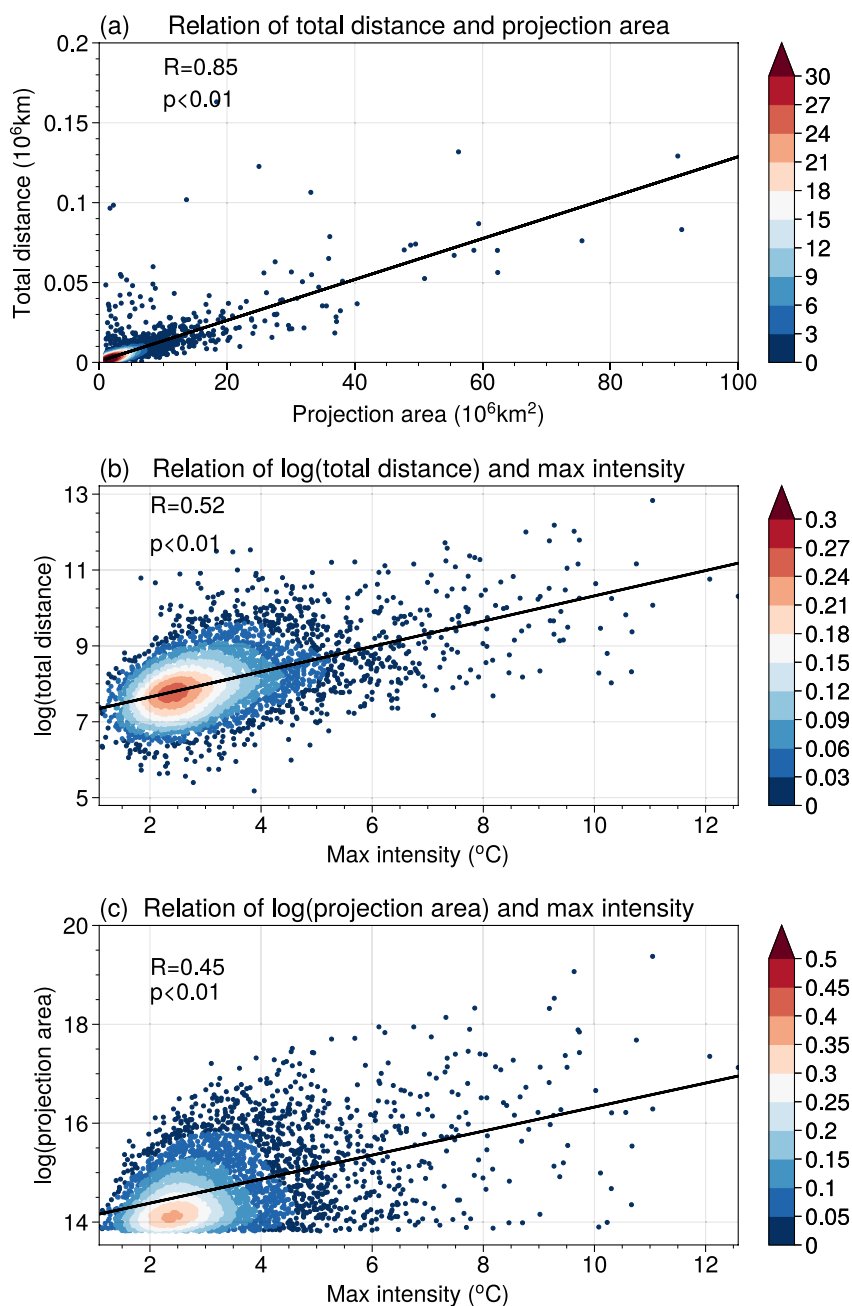


Figure 2. The kernel density distribution of MHW properties. Scatter plots of the total distance and projection area (a), log(total distance) and maximum intensity (b) and log(projection area) and maximum intensity (c) are shown. The black line is the linear regression line for related MHW properties.

layer. In contrast, weaker winds not only promote the occurrence of MHWs across the subtropical region (Gupta et al., 2020) but also trigger wind-evaporation-SST feedback, which can amplify the SST from the subtropical to the central equatorial Pacific (Lorenzo & Mantua, 2016; Oliver et al., 2021). In other words, stronger winds speed up the ocean current, but they may also reduce the SST variability, which could weaken the MHW.

3.3. The Influence of MHW Movement on the Trend of the Projection Area

The influence of the movement of MHWs on the increasing trend of the projection area was further quantified in four categories of MHWs (moderate, strong, severe, and extreme) based on Equation (1). The relative

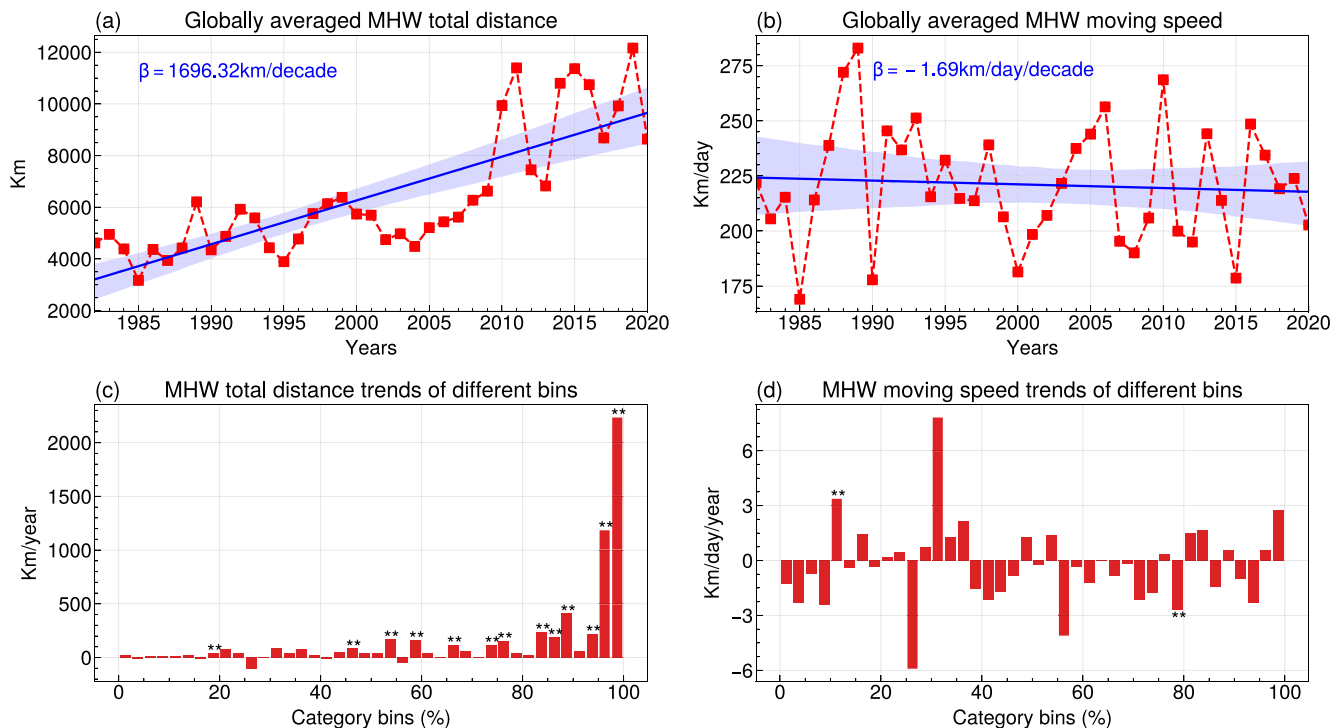


Figure 3. Globally averaged time series of MHW total distance (a) and moving speed (b) over 1982–2020. The blue lines represent the corresponding linear trend. The shaded area indicates the 95% confidence interval of the trend line. In panels (c) and (d), the linear trends (red bars) of total distance and moving speed as a function of the 40 percentile bins during 1982–2020 globally. The double star indicates statistical significance exceeding 95%.

contributions of the frequency and mean projection area in each category to the total projection area are further investigated by a weighted-averaged framework.

Overall, the MHW projection area is heavily influenced by extreme events, which contribute an increase of 0.9 million $\text{km}^2/\text{decade}$ (81.8%) to the increasing trend of the MHW projection area (Figure 4d). For the extreme category, the area term dominates the increase in the projection area, with a contribution of 0.93 million $\text{km}^2/\text{decade}$ (84.7%). However, the frequency term contributes to the decrease in the projection area, with a contribution of -0.03 million $\text{km}^2/\text{decade}$ (-3%) (Figure 4d). The severe category contributes 0.03 million $\text{km}^2/\text{decade}$ (3%) to the increase in projection area (Figure 4c). Interestingly, the area term and frequency term have opposite contributions in the severe category, contributing to 0.23 million $\text{km}^2/\text{decade}$ and -0.2 million $\text{km}^2/\text{decade}$ of the projection area, respectively (Figure 4c). For the moderate category and strong category, the frequency term and area term both contribute to the increase in projection area. The frequency term (1.9%) contributes more than the area term (0.6%) in the moderate category (Figure 4a); however, the frequency term (5.9%) contributes less than the area term (7.8%) in the severe category (Figure 4b). Due to the law of distribution of the projection area, in which small area events are more frequent than large area events (Figure S3g in Supporting Information S1) (Scannell et al., 2016), the frequency term contributes much more than the area term. A similar analysis to the increasing trend of the total area was investigated and obtained a consistent result, with the extreme category contributing the most (detailed description Text S2 and Figure S4 in Supporting Information S1).

4. Conclusion

This article presents an approach to characterize the spatiotemporally contiguous MHW and analyzes the duration, frequency, intensity, area, and movement metrics from a three-dimensional perspective during 1982–2020. This algorithm identifies 3843 MHW events globally and discovers that the MHW duration, maximum intensity, total magnitude, projection area, total area, and moving distance all increase significantly, while the MHW frequency, area mean intensity, and moving speed do not show a significant trend. Further investigation into the response of movement metrics and area metrics under global warming indicates that different intensities of

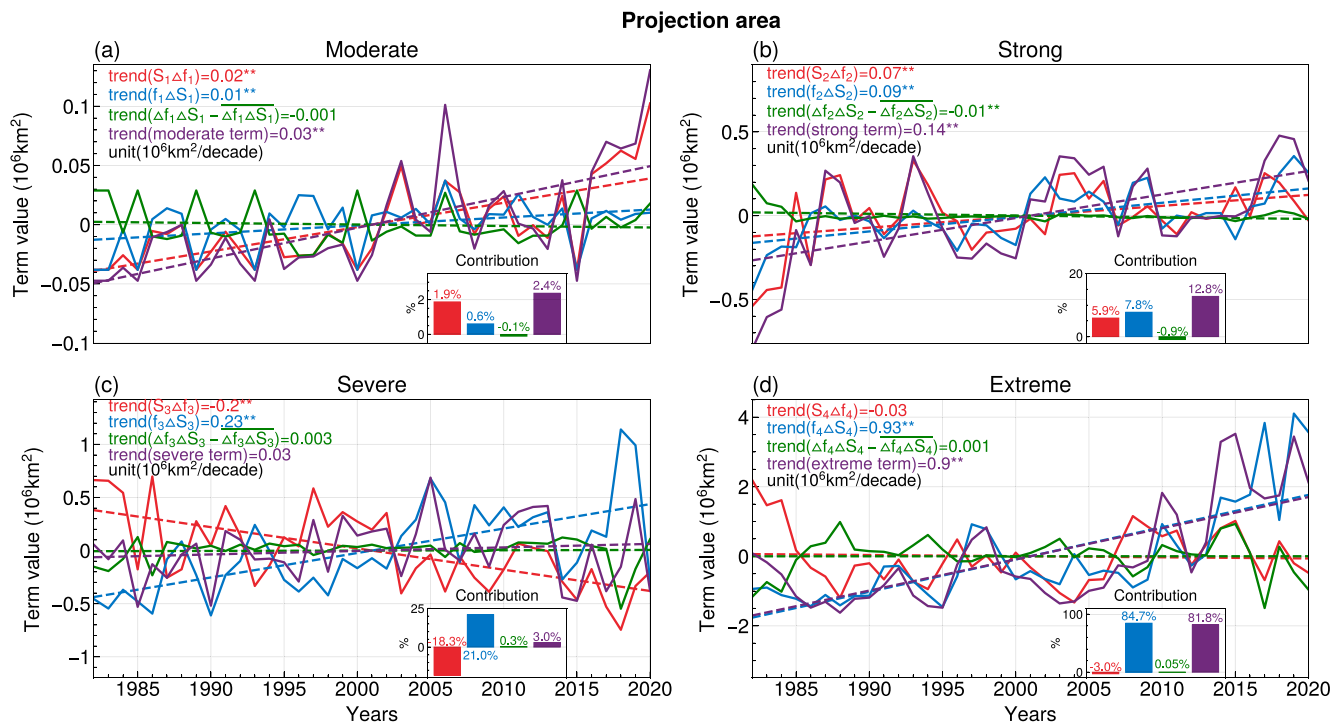


Figure 4. Decomposition of projection area trends for moderate (a), strong (b), severe (c) and extreme (d) categories of MHWs during 1982–2020. The red, blue, green and purple colors represent the influence of the frequency term, area term, residual term and total term in each category based on Equation 1, respectively. The dashed lines are the linear regression lines of the corresponding term. The bar plot in the figure is the contribution of three parts to the total projection area trends. The units of trend values are $\text{km}^2/\text{decade}$.

MHWs contribute unevenly to the variation in movement metrics and area metrics. Most of these increases occur in MHW events with greater intensity, indicating that MHW events with greater intensity are associated with longer movements and larger areas of MHWs. Because small-area events occur more frequently than large area events, the increase in the projection area or the total area was driven by the frequency term for moderate MHWs and the area term for strong, severe, and extreme MHWs.

Data Availability Statement

The NOAA OI SST V2 High Resolution Data set are available at <https://psl.noaa.gov/data/gridded/data.noaa.oisst.v2.highres.html>.

Acknowledgments

This work was jointly supported by the National Science Fund for Excellent Young Scholars (41722502), the National Science Foundation of China (42041004 and 42075018), and the Foundation of Gansu Science and Technology Department (21JR7RA529). This work was also supported by the Supercomputing Center of Lanzhou University.

References

- Benthuisen, J. A., Oliver, E. C. J., Feng, M., & Marshall, A. G. (2018). Extreme marine warming across tropical Australia during austral summer 2015/2016. *Journal of Geophysical Research: Oceans*, 123(2), 1301–1326. <https://doi.org/10.1002/2017jc013326>
- Caputi, N., Kangas, M., Denham, A., Feng, M., Pearce, A., Hetzel, Y., & Chandrapavan, A. (2016). Management adaptation of invertebrate fisheries to an extreme marine heat wave event at a global warming hot spot. *Ecology and Evolution*, 6(11), 3583–3593. <https://doi.org/10.1002/ece3.2137>
- Cheung, W. W. L., & Frölicher, T. L. (2020). Marine heatwaves exacerbate climate change impacts for fisheries in the northeast Pacific. *Scientific Reports*, 10(1), 6678. <https://doi.org/10.1038/s41598-020-63650-z>
- Du, M., Kleidon, A., Sun, F., Renner, M., & Liu, W. (2020). Stronger global warming on nonrainy days in observations from China. *Journal of Geophysical Research: Atmospheres*, 125(10). <https://doi.org/10.1029/2019jd031792>
- Elzahaby, Y., Schaeffer, A., Roughan, M., & Delaux, S. (2021). Oceanic circulation drives the deepest and longest marine heatwaves in the East Australian current system. *Geophysical Research Letters*, 48(17). <https://doi.org/10.1029/2021gl094785>
- Fang, B., & Lu, M. (2020). Heatwave and blocking in the northeastern Asia: Occurrence variability, and association. *Journal of Geophysical Research: Atmospheres*, 125(6). <https://doi.org/10.1029/2019jd031627>
- Frölicher, T. L., Fischer, E. M., & Gruber, N. (2018). Marine heatwaves under global warming. *Nature*, 560(7718), 360–364. <https://doi.org/10.1038/s41586-018-0383-9>
- Galli, G., Solidoro, C., & Lovato, T. (2017). Marine heat waves hazard 3D Maps and the risk for LOW motility organisms in a warming Mediterranean Sea. *Frontiers in Marine Science*, 4. <https://doi.org/10.3389/fmars.2017.00136>

- Gupta, A. S., Thomsen, M., Benthuyens, J. A., Hobday, A. J., Oliver, E., Alexander, L. V., et al. (2020). Drivers and impacts of the most extreme marine heatwave events. *Scientific Reports*, 10(1), 19359. <https://doi.org/10.1038/s41598-020-75445-3>
- Hobday, A., Oliver, E., Gupta, A. S., Benthuyens, J., Burrows, M., Donat, M., et al. (2018). Categorizing and naming marine heatwaves. *Oceanography*, 31(2). <https://doi.org/10.5670/oceanog.2018.205>
- Hobday, A. J., Alexander, L. V., Perkins, S. E., Smale, D. A., Straub, S. C., Oliver, E. C. J., et al. (2016). A hierarchical approach to defining marine heatwaves. *Progress in Oceanography*, 141, 227–238. <https://doi.org/10.1016/j.pocean.2015.12.014>
- Holbrook, N. J., Hernaman, V., Koshiba, S., Lako, J., Kajtar, J. B., Amosa, P., & Singh, A. (2022). Impacts of marine heatwaves on tropical Western and central Pacific Island nations and their communities. *Global and Planetary Change*, 208, 103680. <https://doi.org/10.1016/j.gloplacha.2021.103680>
- Holbrook, N. J., Scannell, H. A., Gupta, A. S., Benthuyens, J. A., Feng, M., Oliver, E. C. J., et al. (2019). A global assessment of marine heatwaves and their drivers. *Nature Communications*, 10(1), 2624. <https://doi.org/10.1038/s41467-019-10206-z>
- Hu, S., Sprintall, J., Guan, C., McPhaden, M. J., Wang, F., Hu, D., & Cai, W. (2020). Deep-reaching acceleration of global mean ocean circulation over the past two decades. *Science Advances*, 6(6). <https://doi.org/10.1126/sciadv.aax7727>
- Hughes, T. P., Kerry, J. T., Álvarez-Noriega, M., Álvarez-Romero, J. G., Anderson, K. D., Baird, A. H., et al. (2017). Global warming and recurrent mass bleaching of corals. *Nature*, 543(7645), 373–377. <https://doi.org/10.1038/nature21707>
- Hughes, T. P., Kerry, J. T., Connolly, S. R., Baird, A. H., Eakin, C. M., Heron, S. F., et al. (2018). Ecological memory modifies the cumulative impact of recurrent climate extremes. *Nature Climate Change*, 9(1), 40–43. <https://doi.org/10.1038/s41558-018-0351-2>
- Jacox, M. G., Alexander, M. A., Bograd, S. J., & Scott, J. D. (2020). Thermal displacement by marine heatwaves. *Nature*, 584(7819), 82–86. <https://doi.org/10.1038/s41586-020-2534-z>
- Liang, Y.-C., Yu, J.-Y., Saltzman, E. S., & Wang, F. (2017). Linking the tropical northern hemisphere pattern to the Pacific warm blob and Atlantic cold blob. *Journal of Climate*, 30(22), 9041–9057. <https://doi.org/10.1175/jcli-d-17-0149.1>
- Liu, K., Xu, K., Zhu, C., & Liu, B. (2022). Diversity of marine heatwaves in the South China Sea regulated by ENSO phase. *Journal of Climate*, 35(2), 877–893. <https://doi.org/10.1175/jcli-d-21-0309.1>
- Lorenzo, E. D., & Mantua, N. (2016). Multi-year persistence of the 2014/15 North Pacific marine heatwave. *Nature Climate Change*, 6(11), 1042–1047. <https://doi.org/10.1038/nclimate3082>
- Luo, M., Lau, N.-C., Liu, Z., Wu, S., & Wang, X. (2022). An observational investigation of spatiotemporally contiguous heatwaves in China from a 3D perspective. *Geophysical Research Letters*, 49(6). <https://doi.org/10.1029/2022gl097714>
- Luo, M., Wang, X., Dong, N., Zhang, W., Li, J., Wu, S., et al. (2022b). Two different propagation patterns of spatiotemporally contiguous heatwaves in China. *NPJ Climate and Atmospheric Science*, 5(1), 89. <https://doi.org/10.1038/s41612-022-00313-y>
- Manta, G., Mello, S., Trinchin, R., Badagian, J., & Barreiro, M. (2018). The 2017 record marine heatwave in the Southwestern Atlantic Shelf. *Geophysical Research Letters*, 45(22), 12449–12456. <https://doi.org/10.1029/2018gl081070>
- Mills, K., Pershing, A., Brown, C., Chen, Y., Chiang, F.-S., Holland, D., et al. (2013). Fisheries management in a changing climate: Lessons from the 2012 ocean heat wave in the Northwest Atlantic. *Oceanography*, 26(2). <https://doi.org/10.5670/oceanog.2013.27>
- Mohanty, P. C., Kushabaha, A., Mahendra, R. S., Nayak, R. K., Sahu, B. K., Rao, E. P. R., & Kumar, T. S. (2021). Persistence of marine heat waves for coral bleaching and their spectral characteristics around Andaman coral reef. *Environmental Monitoring and Assessment*, 193(8), 491. <https://doi.org/10.1007/s10661-021-09264-y>
- Neal, E., Huang, C. S. Y., & Nakamura, N. (2022). The 2021 Pacific northwest heat wave and associated blocking: Meteorology and the role of an upstream cyclone as a diabatic source of wave activity. *Geophysical Research Letters*, 49(8). <https://doi.org/10.1029/2021gl097699>
- Oliver, E. C. J., Benthuyens, J. A., Bindoff, N. L., Hobday, A. J., Holbrook, N. J., Mundy, C. N., & Perkins-Kirkpatrick, S. E. (2017). The unprecedented 2015/16 Tasman Sea marine heatwave. *Nature Communications*, 8(1), 16101. <https://doi.org/10.1038/ncomms16101>
- Oliver, E. C. J., Benthuyens, J. A., Darmaraki, S., Donat, M. G., Hobday, A. J., Holbrook, N. J., et al. (2021). Marine heatwaves. *Annual Review of Marine Science*, 13(1), 313–342. <https://doi.org/10.1146/annurev-marine-032720-095144>
- Oliver, E. C. J., Burrows, M. T., Donat, M. G., Gupta, A. S., Alexander, L. V., Perkins-Kirkpatrick, S. E., et al. (2019). Projected Marine heatwaves in the 21st century and the potential for ecological impact. *Frontiers in Marine Science*, 6. <https://doi.org/10.3389/fmars.2019.00734>
- Oliver, E. C. J., Donat, M. G., Burrows, M. T., Moore, P. J., Smale, D. A., Alexander, L. V., et al. (2018). Longer and more frequent marine heatwaves over the past century. *Nature Communications*, 9(1), 1324. <https://doi.org/10.1038/s41467-018-03732-9>
- Pearce, A. F., & Feng, M. (2013). The rise and fall of the marine heat wave off Western Australia during the summer of 2010/2011. *Journal of Marine Systems*, 111–112, 139–156. <https://doi.org/10.1016/j.jmarsys.2012.10.009>
- Pietri, A., Colas, F., Mogollon, R., Tam, J., & Gutierrez, D. (2021). Marine heatwaves in the Humboldt current system: From 5-day localized warming to year-long El Niños. *Scientific Reports*, 11(1), 21172. <https://doi.org/10.1038/s41598-021-00340-4>
- Reddy, P. J., Perkins-Kirkpatrick, S. E., & Sharples, J. J. (2021). Interactive influence of ENSO and IOD on contiguous heatwaves in Australia. *Environmental Research Letters*, 17(1), 014004. <https://doi.org/10.1088/1748-9326/ac3e9a>
- Reynolds, R. W., Smith, T. M., Liu, C., Chelton, D. B., Casey, K. S., & Schlax, M. G. (2007). Daily high-resolution-blended analyses for sea surface temperature. *Journal of Climate*, 20(22), 5473–5496. <https://doi.org/10.1175/2007jcli1824.1>
- Scannell, H. A., Pershing, A. J., Alexander, M. A., Thomas, A. C., & Mills, K. E. (2016). Frequency of marine heatwaves in the North Atlantic and North Pacific since 1950. *Geophysical Research Letters*, 43(5), 2069–2076. <https://doi.org/10.1002/2015gl067308>
- Schwierz, C., Croci-Maspoli, M., & Davies, H. C. (2004). Perspicacious indicators of atmospheric blocking. *Geophysical Research Letters*, 31(6). <https://doi.org/10.1029/2003gl019341>
- Smale, D. A., Wernberg, T., Oliver, E. C. J., Thomsen, M., Harvey, B. P., Straub, S. C., et al. (2019). Marine heatwaves threaten global biodiversity and the provision of ecosystem services. *Nature Climate Change*, 9(4), 306–312. <https://doi.org/10.1038/s41558-019-0412-1>
- Sparnocchia, S., Schiano, M. E., Picco, P., Bozzano, R., & Cappelletti, A. (2006). The anomalous warming of summer 2003 in the surface layer of the Central Ligurian Sea (Western Mediterranean). *Annales Geophysicae*, 24(2), 443–452. <https://doi.org/10.5194/angeo-24-443-2006>
- Steinfeld, D., Boettcher, M., Forbes, R., & Pfahl, S. (2020). The sensitivity of atmospheric blocking to upstream latent heating numerical experiments. *Weather and Climate Dynamics*, 1(2), 405–426. <https://doi.org/10.5194/wcd-1-405-2020>
- Steinfeld, D., & Pfahl, S. (2019). The role of latent heating in atmospheric blocking dynamics: A global climatology. *Climate Dynamics*, 53(9–10), 6159–6180. <https://doi.org/10.1007/s00382-019-04919-6>
- Steinfeld, D., Sprenger, M., Beyerle, U., & Pfahl, S. (2022). Response of moist and dry processes in atmospheric blocking to climate change. *Environmental Research Letters*, 17(8), 084020. <https://doi.org/10.1088/1748-9326/ac81af>
- Vogel, M. M., Zscheischler, J., Fischer, E. M., & Seneviratne, S. I. (2020). Development of future heatwaves for different hazard thresholds. *Journal of Geophysical Research: Atmospheres*, 125(9). <https://doi.org/10.1029/2019jd032070>

- Walker, H. J., Hastings, P. A., Hyde, J. R., Lea, R. N., Snodgrass, O. E., & Bellquist, L. F. (2020). Unusual occurrences of fishes in the Southern California Current System during the warm water period of 2014/2018. *Estuarine, Coastal and Shelf Science*, 236, 106634. <https://doi.org/10.1016/j.ecss.2020.106634>
- Wernberg, T., Bennett, S., Babcock, R. C., Bettignies, T. d., Cure, K., Depczynski, M., et al. (2016). Climate-driven regime shift of a temperate marine ecosystem. *Science*, 353(6295), 169–172. <https://doi.org/10.1126/science.1248745>
- Wernberg, T., Smale, D. A., Tuya, F., Thomsen, M. S., Langlois, T. J., Bettignies, T. d., et al. (2012). An extreme climatic event alters marine ecosystem structure in a global biodiversity hotspot. *Nature Climate Change*, 3(1), 78–82. <https://doi.org/10.1038/nclimate1627>
- Yao, Y., & Wang, C. (2021). Variations in summer marine heatwaves in the south China sea. *Journal of Geophysical Research: Oceans*, 126(10). <https://doi.org/10.1029/2021jc017792>